ICAS-98-2,4,5

A98-31506

AERODYNAMIC CHARACTERISTICS OF AXISYMMETRIC AND THREE–DIMENSIONAL BODIES AT TRANSONIC SPEEDS

A.S.Fonarev, M.A.Naida
Central Aerohydrodynamic Institute (TsAGI), 140160 Zhukovsky-3, Moscow region, Russia.

Abstract

Theoretical study of steady and unsteady transonic flows about axisymmetric and 3D elongated bodies has been carried out within the framework of non-linear small disturbance theory. Flow unsteadiness can be caused by disturbances of different nature: abrupt changes of flow velocity, ongoing shock waves, etc.

To solve the problem the domain, where the solution is sought, is divided into two regions: inner and outer. By using numerical methods the solutions for boundary value problems in both regions have been obtained and procedure of their matching has been applied.

Special attention has been paid to the problem of wave drag. A formula for calculating wave drag of axisymmetric and 3D bodies has been obtained. For this to be done, the integral form of the momentum equation has been employed. As a result, wave drag value is obtained by integrating velocity jump along shocks closing local supersonic zones. The formula for wave drag is the generalization of the Cole-Murman's one for steady transonic flow about an airfoil and a wing.

Aerodynamic characteristics of some axisymmetric, elongated bodies and a fuselage-swept wing-tail configuration are analyzed. The results are compared with experimental data.

Introduction

When transonic flows about slender bodies of revolution, thin wings with moderate aspect ratio and their combination with fuselage, the maximum cross-section size of which is small in comparison with its length, are considered within the framework of small disturbance theory, the significant problem simplification can be achieved through the use of asymptotic matching solutions technique [1,2]. As it was shown in [1] there are two regions, flows in which are governed by different boundary-value problems. In the inner (adjacent to body) region the main term of the disturbed potential satisfies Laplace equation in perpendicular to body planes. In the outer region at large distance from the body the solution has axisymmetric pattern and its main term coincides with the solution for the equivalent body of revolution.

Thus, the solution for 3D flow problem can be obtained by simultaneous solving two boundary-value problems with unknown functions depending on two spatial variables. Unfortunately, in this case one can not obtain lift of a vehicle: because of axial symmetry of the external flow it is equal to zero. As a result, this approach is employed basically to determine pressure distribution over the surface of the vehicles that have small lift [2].

To simulate transonic flow about a vehicle having lifting wing with high aspect ratio, the new problem statement, which is free of aforementioned drawback, was proposed in [3]. Pursuant to [3] the inner region, the flow in which is governed by Laplace equation in perpendicular to body planes, contains not the whole vehicle but the fuselage with the tail and a part of the wing only. The rest of the wing is placed in the outer region the disturbed potential in which satisfies 3D Karman equation. When using this approach, the integral aerodynamic characteristics of a vehicle are determined by integrating pressure distribution over the body surface in both regions and summarizing the results obtained.

One of the difficult problem of transonic aerodynamics is determination of wave drag of bodies. The point is that the usual method of pressure distribution integration over the body surface is rather inaccurate and can often lead even to negative values for the drag coefficient when the problem is solved numerically within the framework of small disturbance theory [4,5]. In these papers another approach based on the integral form of the momentum equation was proposed and transonic flows about thin airfoils were considered. The method can be readily modified for thin wings, but its immediate reduction to slender bodies of revolution could not be realized because of axisymmetric flow pattern and non-linear relationship between pressure and velocity components in the framework of small disturbance theory. Therefore, in axisymmetric case the problem was resolved

only recently [6]. As a result, the possibility arose to calculate wave drag of 3D configurations comprising wing and fuselage on the basis of both transonic equivalence rule and 3D transonic small disturbance theory. These results are given in this paper. It is worth mentioning [7] where the efficient numerical approximate factorization method to simulate 3D transonic flow about a wing in the framework of small disturbance theory was proposed. In this paper the numerical solution to 3D Karman equation has been obtained by using the approximate factorization method as well.

In [8,9] the integral method was modified for unsteady 2D transonic flow and integral aerodynamic characteristics of an airfoil versus time were obtained in the cases of gusts and moving shocks. The modification of the method for unsteady transonic flow about slender bodies of revolution is given below.

In this paper the consideration is given to the problem of determination of integral aerodynamic characteristics of slender bodies of revolution and vehicles at transonic speeds. The approximate methods of their calculation, based on application of non-linear small disturbance theory, have been developed for axisymmetric and 3D flows. The method used consists in dividing the whole flow domain into two regions (inner and outer), applying numerical methods in both regions and matching the solutions obtained to each other. The Murman-Cole's formula to calculate inviscid drag of an isolated wing has been modified for slender bodies of revolution and fuselage-wing combinations. The data on wave drag of slender bodies of revolution and aerodynamic characteristics (inviscid drag, lift and pitching moment) of the vehicle consisting of fuselage, swept wing and tail have been obtained. Their comparison with experimental ones has been fulfilled.

Wave drag of bodies of revolution

Problem statement

In the framework of small disturbance theory the axisymmetric unsteady transonic flow about a slender body of revolution is governed by the following equation:

$$M_\infty^2 \varphi_{tt} + 2 M_\infty^2 \varphi_{xt} = ((C_1 + C_2 \varphi_x)\varphi_x)_x + \frac{1}{r}\left(r \varphi_r\right)_r \quad (1.1)$$

where $C_1 = 1 - M_\infty^2$, $C_2 = -(\gamma+1) M_\infty^2/2$.

As boundary conditions at infinity for (1.1) the so-called non-reflecting conditions, which can be derived from the relation held on the characteristic surface, are applied. The equation for the characteristic surface has the form:

$$M_\infty^2 \xi_t^2 + 2 M_\infty^2 \xi_x \xi_t = C \xi_x^2 + \xi_r^2, \quad (1.2)$$

$$C = C_1 + 2 C_2 \varphi_x$$

the solution to (1.2) can be written as follows:

$$\xi = \sqrt{x^2/C + r^2} - \sqrt{C}\, t \Big/ \left(M_\infty \sqrt{C + M_\infty^2}\right) -$$

$$- M_\infty x \Big/ \left(\sqrt{C}\sqrt{C + M_\infty^2}\right)$$

Corresponding relation on the characteristic surface assumes the form:

$$-\frac{x\varphi_x}{d} - \frac{r\varphi_r}{d} + \left(\frac{M_\infty^2 x}{Cd} - M_\infty \sqrt{\frac{C + M_\infty^2}{C}}\right)\varphi_t = 0,$$

$$d = \sqrt{x^2/C + r^2}.$$

The asymptotic form of this expression as $x \to \pm\infty$, $y \to \infty$ yields boundary conditions on the left-hand side, right-hand side and upper boundaries respectively:

$$C\varphi_x - M_\infty\left(M_\infty + \sqrt{C + M_\infty^2}\right)\varphi_t = 0, \quad x \to -\infty \quad (1.3)$$

$$C\varphi_x - M_\infty\left(M_\infty - \sqrt{C + M_\infty^2}\right)\varphi_t = 0, \quad x \to \infty \quad (1.4)$$

$$M_\infty \varphi_r + \sqrt{C}\sqrt{C + M_\infty^2}\,\varphi_x = 0 \qquad r \to \infty \quad (1.5)$$

Unlike the 2D plane case, flow tangency condition can not be assigned to the line $r=0$ because of singularity. To avoid it, the solution is sought in two regions: inner ($0 < r \le r_*$, r_* is rather small) and outer: ($r_* < r$). The solution in the inner region that satisfies flow tangency condition on the surface of the slender body of revolution described by equation $r=R(x)$, $-0.5 \le x \le 0.5$ has the form $r\varphi_r = R R_x$. Thus, the boundary condition on the lower boundary can be written as:

$$\varphi_r = S_x / 2\pi r, \quad r = r_* \quad (1.6)$$

here $S(x)$ - the area of cross-section of the body.

To solve the problem in the outer region, the alternating direction method with first-order accurate monotone Engquist-Osher scheme [10] modified for axisymmetric case [6] is employed.

Determination of wave drag of bodies

The inviscid drag of a slender body of revolution can be written in the form of the integral:

$$c_d = 2\pi \int_{-0.5}^{0.5} c_p R R_x \, dx$$

where $c_p = -2u - v^2$

In the inner region $u = \varphi_x = S_\infty \ln r / 2\pi + g_x$, $g(x)$ - an arbitrary function which can be obtained from the solution in the outer region. Velocity and pressure on the body surface are given by:

$$u = u_* + \frac{S_\infty}{2\pi}\ln\frac{R}{r_*}, \qquad c_p = -2\left(u_* + \frac{S_\infty}{2\pi}\ln\frac{R}{r_*}\right) - R_x^2$$

where subscript * means value at $r = r_*$.

Drag coefficient consists of two terms:

$$c_d = c_{d1} + c_{d2}, \quad c_{d1} = 4\pi\int_{-0.5}^{0.5} u_* v_* r_* dx,$$

$$c_{d2} = -2\pi\int_{-0.5}^{0.5}\left(\frac{S_\infty}{\pi}\ln\frac{R}{r_*} + R_x^2\right) R R_x dx \qquad (1.7)$$

The first term can be recast by applying the integral theorem of momentum to the combination of Karman equation and no-vorticity equation written in the form of conservation law:

$$\left(r C_1\frac{u^2}{2} + 2r C_2\frac{u^3}{3} - r\frac{v^2}{2}\right)_x + (ruv)_r = 0 \qquad (1.8)$$

Integrating (1.8) over the outer region Ω (fig.1) and applying Green's theorem yield a relation in the form of a curvilinear integral along the boundary:

$$\oint\left[r\left(C_1\frac{u^2}{2} + 2C_2\frac{u^3}{3} - \frac{v^2}{2}\right)\right]dr - ruvdx = 0$$

By applying a number of mathematical transformations analogous to those in the case of 2D plane flow [4], we obtain:

$$c_{d1} = \frac{\pi(\gamma+1)}{3} M_\infty^2 \int_{sh} r[u]^3 dr$$

Subscript sh means integration along shocks, square brackets - jump of a value across a shock. Note that this integral is always positive.

For the second term c_{x2}, depending only on the body shape, the integral can be calculated in general:

$$c_{d2} = -\frac{(S_\infty)^2}{2\pi}\ln\frac{R}{r_*}\Big|_{-0.5}^{0.5}$$

For thin closed bodies $c_{x2} \to 0$ as $R \to 0$ at $x = \pm 0.5$; if $R \neq 0$ at $x = 0.5$ this term differs from zero.

Results of numerical simulation

Fig.2 presents steady wave drag versus free stream Mach number for the body of revolution consisting of elliptical forebody, cylindrical midbody and ogive aftbody. The thickness ratio of the body δ is equal to 0.1. The curve denoted by number 1 corresponds to calculation in

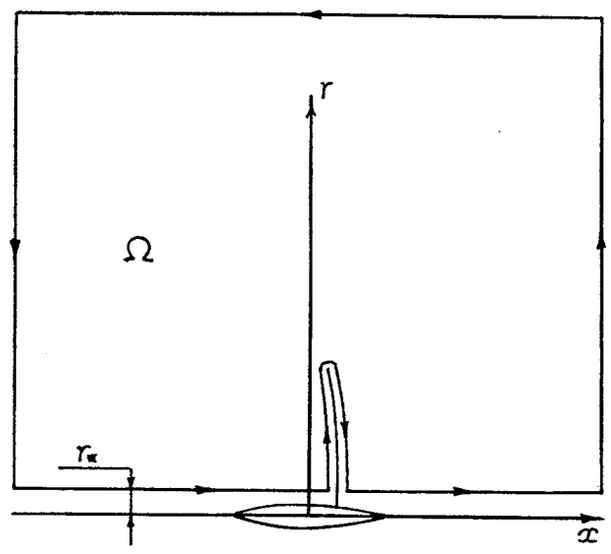

Fig.1 Axisymmetric flow, inner and outer regions, contour of integration.

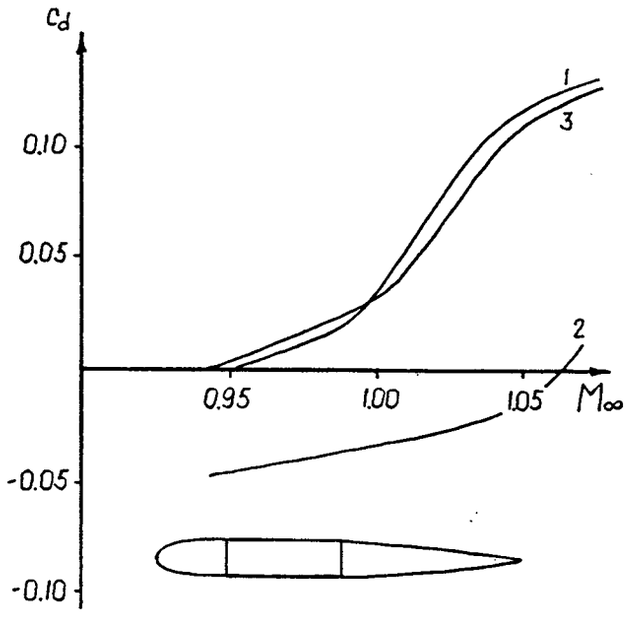

Fig.2 Wave drag of a body of revolution, δ=0.1. 1-integration along shocks, 2-integration over the body surface, 3-experiment (TsAGI)

accordance with (1.7), 2 - calculation by means of pressure distribution integration over the body surface, 3 - experimental results obtained by K.P.Petrov at TsAGI. As it is seen, pressure integration over the body surface leads to negative values of wave drag.

Fig.3 shows steady wave drag versus free stream Mach number for the body of revolution that corresponds in the framework of transonic equivalence rule to a schematic vehicle.

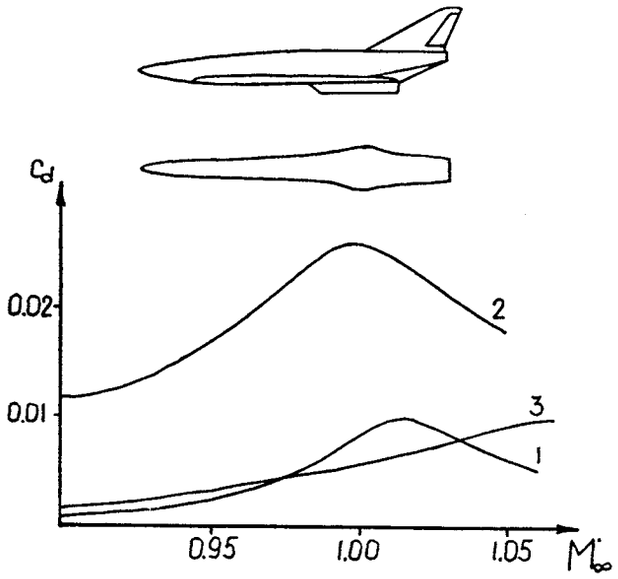

Fig.3 Wave drag of a schematic vehicle, transonic equivalence rule. 1-integration along shocks, 2-integration over the surface of the equivalent body of revolution, 3-experiment (TsAGI).

Fig.4 demonstrates how wave drag of the body shown in fig.2 changes in time at sudden entry into a horizontal gust. The initial Mach number $M_\infty = 0.93$, after the entry $M_\infty = 0.98$. Curve denoted by number 1 means integration along shocks, 2 - over the body surface (note that the curve gives negative value for steady wave drag).

The change of wave drag in time in the case of shock wave reaching the body from behind is shown in fig.5, designatory numbers having the same meaning as those in fig.4. Curve 1 (integration along shocks) exhibits non-monotone behaviour, assumes negative values (the shock pushes the body from behind) but eventually tends to correct steady value (zero, since the flow about the body becomes sub-critical when the moving shock leaves the body and goes upstream). Curve 2 eventually assumes negative steady value i.e. - propulsion. Integration along shocks has been done using the following formula [11]:

$$c_d(t) = \frac{\pi(\gamma+1)}{3} M_\infty^2 \int_{sh} r[u]^3 dr - \frac{S_x^2}{2\pi} \ln \frac{R}{r_*} \Big|_{-0.5}^{0.5} +$$

$$+ 4\pi M_\infty^2 \int_h \frac{dx}{dt} r < u > [\varphi_t + 2u] dr +$$

$$+ 4\pi M_\infty^2 \iint_\Omega ru(\varphi_t + 2u)_t dx dr - 4\pi \int_{-0.5}^{0.5} R R_x(\varphi_*)_t dx$$

where <·> means arithmetic mean across a shock.

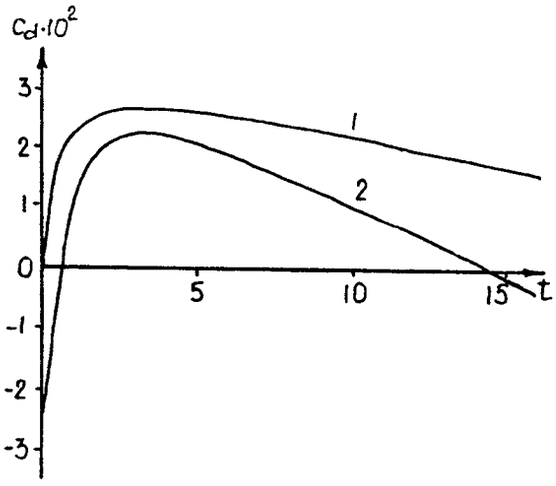

Fig.4 Unsteady wave drag of a body of revolution at entry into a gust. $M_\infty = 0.93$, δ=0.1, ΔM = 0.05. 1-integration along shocks, 2-integration over the body surface

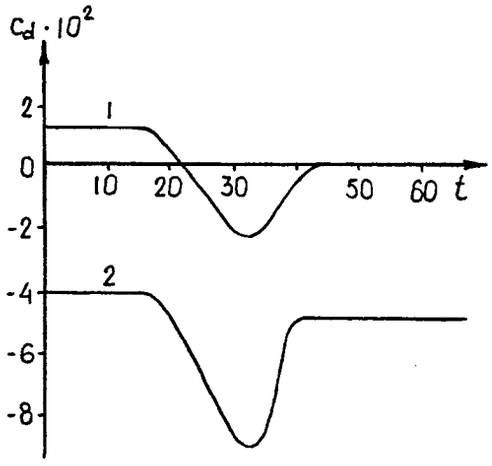

Fig.5 Unsteady wave drag in the case of shock wave reaching the body from behind. $M_\infty = 0.98$, pressure jump across moving shock $\Delta c_p = 0.21$. 1-integration along shocks, 2-integration over the body surface.

Determination of aerodynamic characteristics of a vehicle

Problem statement

Within the framework of transonic small disturbance theory the normalized potential φ satisfies 3D Karman equation, the unsteady analogue of which has the form:

$$M_\infty^2 \varphi_{tt} + 2 M_\infty^2 \varphi_{xt} = ((C_1 + C_2\varphi_x)\varphi_x)_x + \varphi_{yy} + \varphi_{zz} \qquad (2.1)$$

Following [3] we divide the entire flow domain into two regions (fig. 6) the flow in each of which is governed by different boundary value problems.

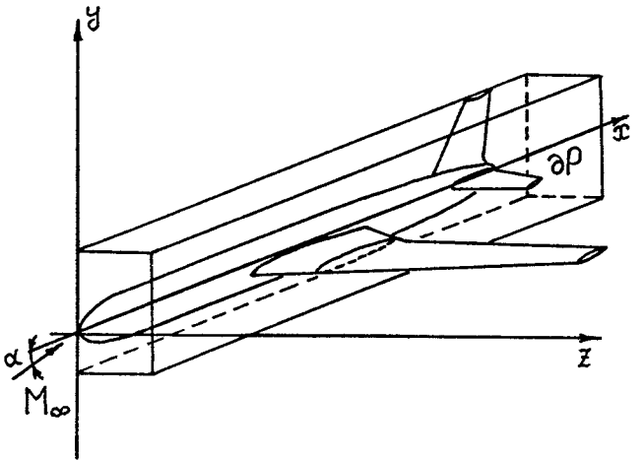

Fig.6 Three-dimensional flow, inner and outer regions.

In the inner, adjacent to body region, which has a form of parallelogram P, the main term of asymptotic expansion of ψ satisfies Laplace equation in $x = const$ planes.

$$\psi_{yy} + \psi_{zz} = 0. \qquad (2.2)$$

Outside P the flow is three dimensional and is described by the potential φ which satisfies (2.1). To match inner and outer solutions to each other the conditions of continuity of the potential and its normal to P derivative are satisfied at the parallelogram surface ∂P:

$$\varphi = \psi, \quad x,y,z \in \partial P; \qquad (2.3)$$

$$\varphi_n = \psi_n, \; x,y,z \in \partial P. \qquad (2.4)$$

On the body surface the potential should satisfy flow tangency condition. For the part of the vehicle inside P:

$$\psi_n = -(N_x + \alpha N_y)/\sqrt{N_y^2 + N_z^2}\,. \qquad (2.5)$$

where N_x and N_y are Cartesian components of the normal unit vector N, α - angle of attack. In the outer region on the wing surface the following conditions hold:

$$\varphi_y = F^+{}_x - \alpha, \qquad y = y_w$$

$y = F^+(x,z)$ are the equations describing the upper and lower wing surfaces respectively, $y = y_w$ is the chord plane. The jump of the potential across vortex sheet is given by:

$$\varphi(x, y_w+0,z) - \varphi(x, y_w-0,z) = [\varphi] = \Gamma(z) \qquad (2.7)$$

where $\Gamma(z)$ - circulation around corresponding wing span station. The vertical component of velocity v is continuous across vortex sheet:

$[\varphi_y] = 0$ at $y = y_w$

Condition (2.7) is the boundary condition for Laplace equation at Treffts plane. In the plane of symmetry $z = 0$ $\psi_z = \varphi_z = 0$. Since the solution is advanced in time, one can employ the same boundary conditions as in the previous section. As a result we have:

$$C\varphi_x - M_\infty(M_\infty + \sqrt{C + M_\infty^2})\varphi_t = 0 \qquad \text{as } x \to -\infty;$$

$$M_\infty\varphi_y - \sqrt{C}\,\sqrt{C + M_\infty^2}\,\varphi_x = 0 \qquad \text{as } y \to -\infty;$$

$$M_\infty\varphi_y + \sqrt{C}\,\sqrt{C + M_\infty^2}\,\varphi_x = 0 \qquad \text{as } y \to \infty;$$

$$M_\infty\varphi_z + \sqrt{C}\,\sqrt{C + M_\infty^2}\,\varphi_x = 0 \qquad \text{as } z \to \infty.$$

When the problem is solved, pressure coefficient in the inner region is determined by: $c_p = -2\psi_x - \psi_y^2 - \psi_z^2$, in the outer $c_p = -2\varphi_x$.

Without making intermediate transformations based on the momentum theorem and analogous to those described in [5] for an isolated wing, we render final result for inviscid drag of a vehicle (subscript tf means integration over Treffts plane):

$$c_{d0} = \frac{\gamma+1}{3} M_\infty^2 \iint_{sh} [u]^3 \, dydz + 2\iint_{tf} \left(v^2 + w^2\right) dydz. \qquad (2.8)$$

The first term is not equal to zero only if there are shocks in the flow. The second term accounts for induced drag which differs from zero if there is lift.

Numerical method

For solving boundary value problem in the inner region the use is made of panel method [2]. Within the framework of this method the contours of cross-sections of the body and parallelepiped P by planes $x=x_i$ are approximated by a set of panels - single layers each of which has constant intensity. Vortex sheet stretching downstream from the trailing edge of the part of the wing that is inside P is approximated by a set of panels - lying in the plane $y = y_w$ double layers with intensity which, according to (2.7), can be found as the jump of potential at the trailing edge. To determine the intensity of single layers boundary conditions are used. To obtain the complete system of linear algebraic equations with dense matrix in any cross-section $x_i = const$, the boundary conditions are satisfied in the center of each single layer. Since the right-hand side vector in this case, according to (2.3) depends on the distribution of potential φ, which, in turn, is advanced in time, the systems of linear equations in the inner region are to be solved many times. The most burdensome stage in solving a system of linear algebraic equations by Gaussian elimination is the transformation of a matrix to upper triangular form. To avoid repeating this stage and increase the solution accuracy, one should resort to alternative method of LU-decomposition with

Fonarev, Naida

pivoting the biggest matrix entries. In this case it suffices to fulfil LU-decomposition only once.

Let us consider the numerical method applied for solving boundary value problem in the outer region. Since the solution is advanced in time, the unsteady terms in (2.1) are retained. To approximate the non-linear part of (2.1) the use is made of monotone first-order accurate Engquist-Osher scheme [10], linear differential operators are approximated by conventional central-difference expressions. The solution to the system of finite-difference equations is obtained by means of approximate factorization method. Within the framework of this method a 3D finite-difference operator is approximated by a product of three one-dimensional ones [13].

Thus, to advance to the next time level, one should solve one system of linear algebraic equations with 4-diagonal matrix (x-sweep) and two systems with 3-diagonal matrices (y and z-sweeps). For solving systems of linear equations with matrices of such pattern when all diagonals are close to the principal one the use is made of scalar sweep. For the scalar sweep to be stable it is required that $|a_{ii}|$ be $\geq \sum_{j=1}^{N} |a_{ij}|$, $j \neq i$ for $1 \leq i \leq N$ where N denotes the number of equations to be solved. When doing y and z-sweeps this inequality is satisfied unconditionally. To ensure that the inequality is satisfied in doing x-sweep, the term $M_\infty^2 \varphi_{tt}$., which is negligible within the framework of small disturbance theory, is retained in equation (2.1).

Results of numerical simulation

Consider the flow about the model of the passenger aircraft shown in fig.7 over a Mach number range of $0.82 \leq M_\infty \leq 0.98$ at two angles of attack $\alpha = 0$ and 4^0. The wing lies in the center plane, has a leading edge sweep $\chi = 37^0$, taper ratio $\eta = 3.64$, aspect ratio $\lambda = 7.58$. Wing sections are symmetrical П–114c airfoils. The tail has symmetrical airfoil NACA0010M as well. The tailplane is mounted at -3^0 to the center line of the fuselage the cross-sections of which are circles.

The pressure coefficient c_p distributions over the wing surface at four span stations (a-d) have been analyzed at $\alpha = 0$ and $M_\infty = 0.95$. The analysis of the data shows that the pressure minimum point is located at 34.1; 38.3; 49.5; 52% of the local chord length from the

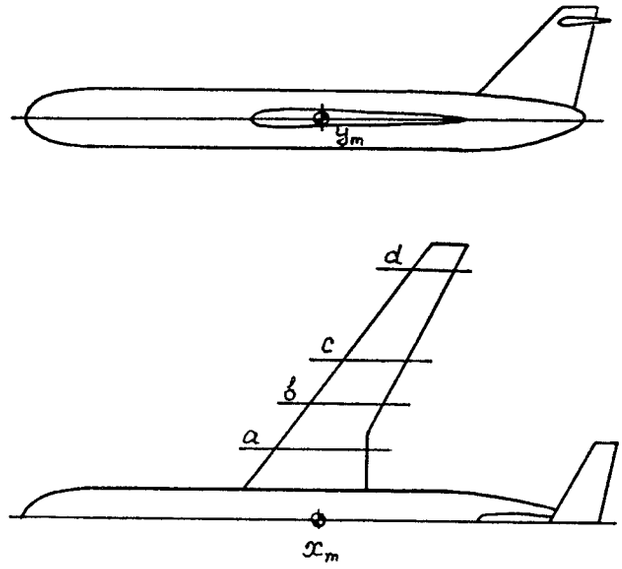

Fig.7 Model of passenger aircraft, wing leading edge sweep $\chi = 37^0$, taper ratio $\eta = 3.64$, aspect ratio $\lambda = 7.58$.

trailing edge at a-d span stations respectively. Thus, at root span stations the low pressure region moves toward the trailing edge, at tip span stations - toward the leading edge. As a result, at root span stations pressure forces acting on forewing increase, on aftwing - decrease. Hence, the drag coefficient at these stations assumes large positive values. At tip span stations the displacement of the low pressure region toward the leading edge accounts for decrease of pressure forces acting on forewing and increase of pressure forces acting on aftwing. Therefore, drag coefficient at these stations decreases down to negative values. At intermediate span stations local drag coefficient varies from positive to negative values. The described behaviour is observed in experiment too [14].

The computational and experimental data on c_d, c_l, c_m versus M_∞ at $\alpha = 0$ are given in fig.8. Curve 1 accounts for c_d, obtained by integration along shocks in accordance with (2.8), curve 2 - experimental results, calculated as full drag at a given Mach number minus full drag at $M_\infty = 0.6$ (subcritical regime), curve 3 - pressure distribution integration over the body surface. The computational lift is given by curve 4. In this case lift is produced mainly by tailplane and has small negative value since the tailplane is mounted at negative angle. The comparison between the computed curve 4 and experimental curve 5 shows that their correlation is rather good except for Mach number range $0.87 \leq M_\infty \leq 0.92$.

The reported discrepancy is attributed, probably, to viscous effects, which are neglected in this study.

Curves 6 and 7 in fig.8 present computational and experimental pitching moment. In both cases pitching moment is determined regarding the model's mass center the position of which is shown in fig.7 (x_m , y_m). Since the fuselage is near-axisymmetric, the wing lies in the centerplane and $y_m = y_w$, pitching moment is produced mainly by aerodynamic forces acting upon the tail. The comparison between computational and experimental curves $c_m(M_\infty)$ makes it possible to draw conclusion that the part of drag produced by viscous forces and not taken into account in this study makes a significant contribution to the resultant pitching moment. Note that the computational curve gives lower values for c_m because viscous forces acting upon the tail produce moment of the same sign as that produced by lift.

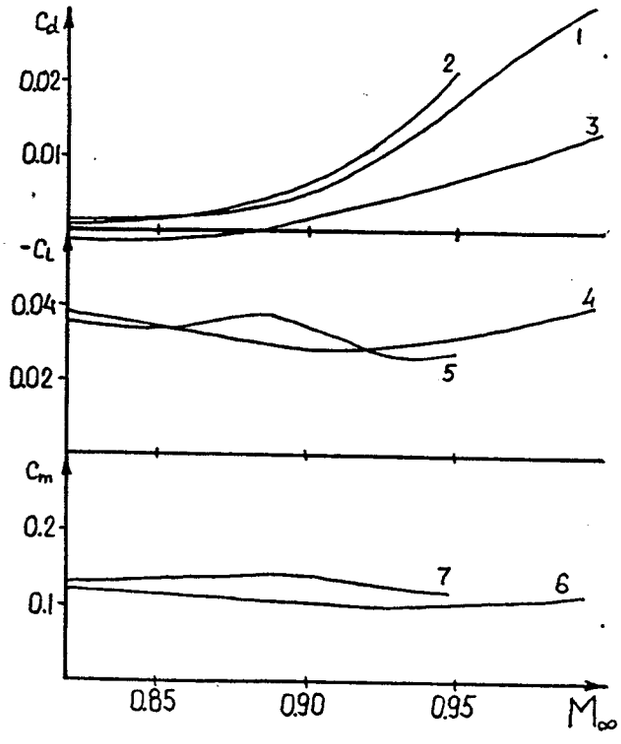

Fig.8 Inviscid drag, lift and pitching moment versus M_∞ at $\alpha = 0^0$. 1-integration over shocks, 2-experiment (TsAGI), 3-integration over the body surface, 4,6-calculation, integration over the body surface, 5,7-experiment (TsAGI).

Computational and experimental aerodynamic characteristics of the model within the system of wind axes versus M_∞ at $\alpha = 4^0$ are given in fig.9. The numbers the curves are denoted by have the same meaning as those in fig.8.

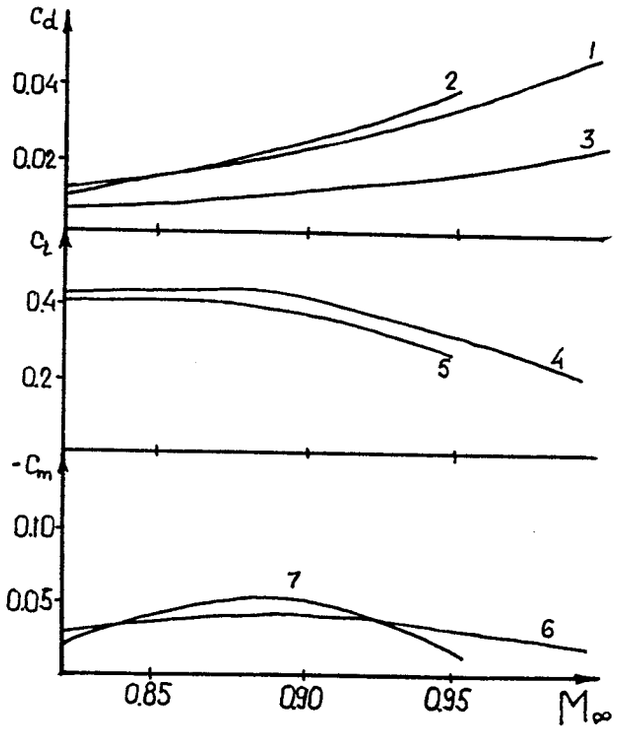

Fig.9 Inviscid drag, lift and pitching moment versus M_∞ at $\alpha = 4^0$. 1-integration over shocks, 2-experiment (TsAGI), 3-integration over the body surface, 4,6-calculation, integration over the body surface, 5,7-experiment (TsAGI).

In this case the wing produces large lift (curves 4 and 5). Hence, the contribution of induced drag to resultant drag should be taken into account in determining experimental values for inviscid drag. Therefore, as differs from the previous case, the inviscid drag presented by curve 2 is calculated as experimental drag at a given Mach number minus difference between resultant experimental and induced drag at $M_\infty = 0.6$. To obtain the latter by using formula (2.8), subcritical flow about the model at $M_\infty = 0.6$ and $\alpha = 4^0$ has been simulated in addition to aforementioned Mach number range.

As a whole, comparison between experimental and computational aerodynamic characteristics of the vehicle makes it possible to infer that their correlation is satisfactory. Note that inviscid drag can be calculated with an adequate accuracy only by integrating along shocks.

Fonarev, Nosko